FINITE ELEMENT ANALYSIS OF THE AXIAL CAPACITY OF MICROPILES

Mohamed. A. Elkasabgy[1], M. Hesham. El Naggar[2]

ABSTRACT

Micropiles are being increasingly utilized in many ground improvement applications to increase the bearing capacity and reduce settlement, particularly for underpinning existing foundations. This paper presents a two dimensional numerical analysis of the behaviour of a single micropile installed in soft clay and subjected to compression loading. The behaviour of soil is simulated using the elastic-perfectly plastic stress-strain relationship incorporated with the Mohr-Coulomb failure criterion. The study also examines the effect of micropile geometrical configurations and interface parameters on the estimated capacity.

Keywords: micropile; axial compressive capacity; inverse analysis; finite element.

[1] Research Assistant & PhD. Candidate, E-mail: melkasab@uwo.ca
[2] Professor & Research Director, Geotechnical Research Centre, Associate Dean, Research and External Relations, E-mail: helnagg@engga.uwo.ca
Address: Faculty of Engineering, University of Western Ontario, London, Ontario, Canada, N6A 5B9, Tel: (519)661-4219, Fax: (519)661-3942.

INTRODUCTION

The micropilling technique has been proven successful in increasing the stiffness of soils, upgrading their safe bearing capacity, and reducing their total and differential settlements. Micropiles are generally used as foundation support elements, structural foundation underpinning, excavation stabilization, and reinforcement of slopes. To illustrate the rapid growing use of micropiles worldwide, valuable overviews have been provided by Mason and Bruce (2001), Juran et al. (1999), Bruce (1989), Bruce (1988), Lizzi (1985), Bruce and Yeung (1983), and Koreck (1978).

Despite their growing use, micropiles methods of design are still preliminary and are based on the state of practice for design of large diameter drilled piles and ground anchors (Bruce and Juran, 1997). These methods may result in a conservative design for micropiles of depth to diameter ratios less than 100 (Jeon, 2004). Some studies of Type B micropiles in clayey soils recommend using the concept of the total stress analysis. In such design method, the shaft resistance is related to the undrained shear strength of soil, C_u, through the adhesion factor α.

Bruce and Juran (1997) recommended using the values of α assigned to Type A micropiles for the design of Type B piles. For guidance, Littlejohn (1980) proposed α values based on gravity-grouted ground anchors results, which have later been incorporated in the British code BS-8081(1988). The suggested values were between 0.3 and 0.35 for stiff London Clay (C_u>90 kPa), 0.28 and 0.36 for stiff over-consolidated clay (C_u=270 kPa), 0.48 and 0.6 for stiff to very stiff marls (C_u=270 kPa), and 0.45 for stiff clayey silt (C_u=95 kPa). Bruce (1994) indicated that gravity-grouted micropiles were often designed satisfactorily with α varied between 0.6 and 0.8. This, however, depicts the significant variation in α reported in literature.

Although the widespread use of these ranges, there was so far no robust method for estimating α. Thus, more work is required to draw a complete picture of the recommended practical ranges of α based on the site soils, micropile construction technique, and grouting pressure. Therefore, more optimized and safe design can be achieved. With the advance in the methods of analysis, this paper is utilizing the powerful finite element method to investigate thoroughly the inherent point of the micropile-soil interface parameters.

OBJECTIVES

The primary objectives of this study are to: practically quantify the adhesion properties of Type B micropiles in soft to medium stiff clays; and evaluate the effect of micropile diameter on the mobilised ultimate resistance and load sharing mechanism. A coupled finite element analysis using a two dimensional nonlinear finite element code, PLAXIS, was performed. The soil behaviour is simulated using an elastoplastic constitutive relation with the non-associated Mohr-Coulomb criterion. The load-settlement records from a full-scale load test (Han and Ye, 2006) are employed to estimate the adhesion factor α.

SITE CHARACTERISTICS AT FIELD LOAD TESTING LOCATION

The soil profile and soil properties of the Shanghai soft clay deposits at the test site are shown in **Fig.1**. The soil profile consists of a thin topsoil layer overlying a lean clay crust (CL), followed by soft lean clay (CL) layer (called mucky clay in China), underlain by a thick fat clay layer (CH). The water table is at 1.0 m from the existing ground surface. The moisture content of the lean clay and fat clay layers is greater than their liquid limit. The shear strength parameters were obtained from consolidated undrained triaxial tests (CU) on undisturbed samples recovered from the test site and field vane shear tests (Han and Ye, 2006).

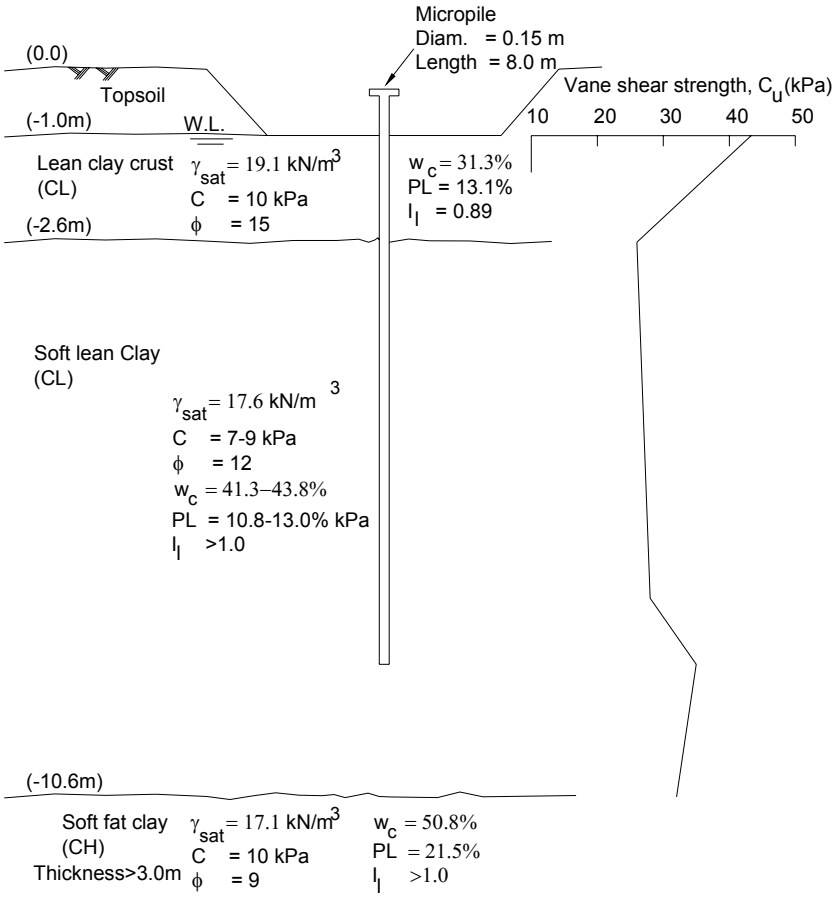

Note: c=total cohesion; I_l=liquidity index; PL=plastic limit; w_c=moisture content; γ_{sat}=saturated unit weight; ϕ=total friction angle.

Figure 1. Soil profile.

A micropile was constructed using a vibratory drilling rig with the aid of jets of water to extend completely through the soft lean clay layer. The nominal diameter and length of micropile were 0.15 m and 8.0 m, respectively. A pressure of 0.2 - 0.5 MPa was applied to the cement grout in the drilled hole, producing a bonded zone along the entire length of the micropile. Accordingly, it may be classified as Type B (Bruce and Juran, 1997). For loading test purposes, the first 1.0 m of the top soil was removed and the quick maintained-load method was adopted to test the micropile, following the ASTM D1143. The loading criterion for the field load procedure was such that an increment of load (10 kN) was added after the previous loading increment was maintained for 1 h.

FINITE ELEMENT MODELLING

The response calculation was accomplished in three phases. First, the gravity load was applied to soil in order to establish the initial stress state prior to micropile installation. Second stage was the micropile construction, simulated by assigning the micropile material properties to its specified region (i.e. replacing the assigned soil properties). This simulation of micropile construction is an abridged idealization to the complicated construction procedures, which are avoided in the current study for simplifying the analysis. Finally, the load increments were applied following the adopted test procedure. Between each two successive load increments, a consolidation stage for a time period of 1 h is specified. These stages have been established based on the geometrical and material modelling explained below.

Geometrical Modelling

The axisymmetrical model was established to simulate the radial cross-section and loading scheme of the tested micropile. A 15-noded triangle element from the PLAXIS element library is utilized, which provides fourth order interpolation for displacements and twelve gauss stress points. This element type is believed to offer high quality stress results and to be adequate for failure situations. The vertical boundaries of the model are assigned to be free and smooth. On the other hand, the base of the model was designed to be rough and rigid. Based on the analytical solution proposed by Randolph and Wroth (1978) to evaluate the deformation of soil around a pile shaft, the model vertical boundary was set at a distance r from the axis of symmetry. The distance r is the radius at which the shear stress becomes negligible, which is computed as follows for frictional piles:

$$r = 2.5L(1 - \nu) \qquad (1)$$

where, L is the micropile length (8.0m) and ν is the undrained Poisson's ratio taken as 0.5. For the adopted micropile length to mean radius ratio, L/r_m=53, where r_m= 0.075 m, the effect of the undrained Poisson's ratio chosen for calculating r is expected to be insignificant on the load-settlement behaviour of

the micropile (Randolph and Wroth, 1978). Consistent with the finite element analysis proposed by the same researchers, the rigid horizontal boundary was imposed at a depth of 2.5 times the micropile length. This implies that the model extends horizontally by 10 m from the axe of symmetry and vertically by 20 m from ground surface. **Figure 2** illustrates the finite element mesh for the modelled micropile. It is observed that the soft lean clay layer is divided into two separate layers, namely: soft lean clay (1) and soft lean clay (2). The thickness of the former is 6.4 m and the latter is 1.6 m. The reason for this discretization is discussed in the material modelling section. It is worth noting that the top soil layer shown in **Fig. 1** is not modelled as it was removed in the field prior to micropile construction.

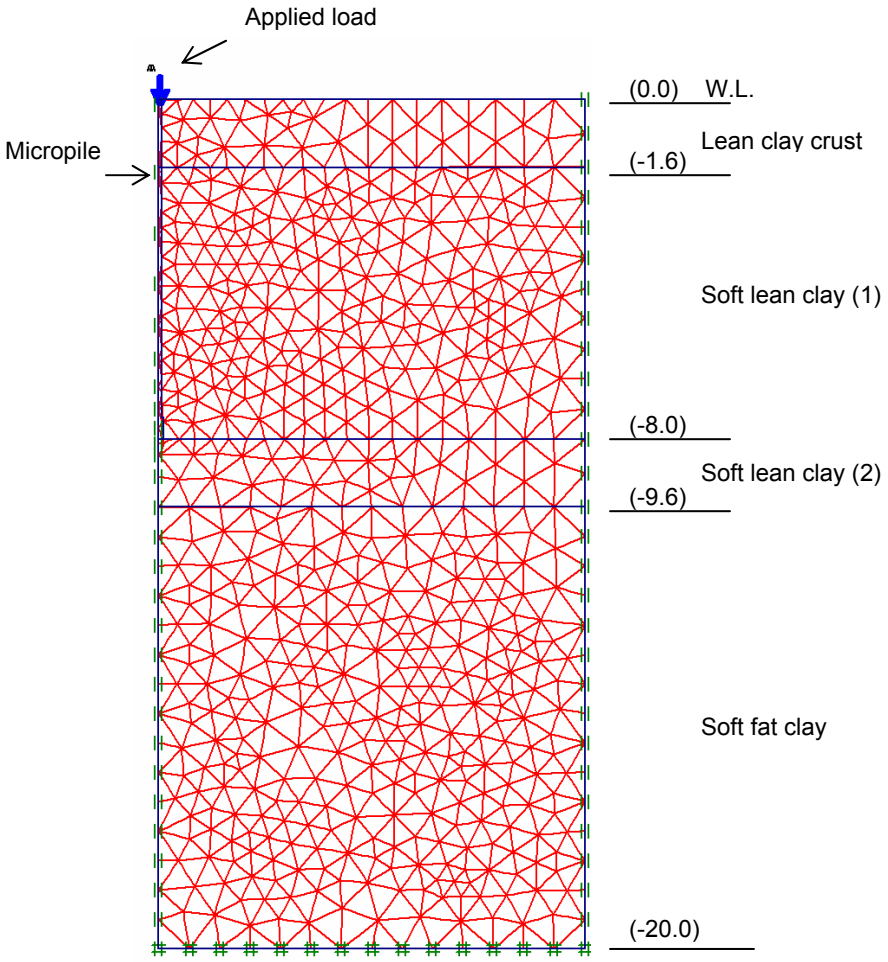

Figure 2. Finite element mesh.

Han and Ye (2006) compared the observed yield load at the pile toe with the theoretical bearing capacity ($9xC_u$) using the approach proposed by Randolph (1994), and concluded that the micropile toe might have been enlarged. Therefore, they attributed that enlargement to the construction method,

which involved washing the slurry out and grouting from the bottom of the hole up in the soft clays. Thus, to achieve a match between the measured toe yielding load and the calculated bearing capacity value, the anticipated diameter of the enlarged portion was estimated to be 0.228 m. Unfortunately, no field measurements were available in the reference study for the actual length and diameter of the enlarged portion. For the purpose of numerical modelling, the diameter of 0.228 m was used to represent based on the aforementioned theoretical evidence. The length of the enlarged portion length, l_{en}, is estimated, and three different values (0.25, 0.5, and 1.0 m) are considered to investigate their influence on the simulated micropile response.

Material Modelling

The material parameters of the three modelled soil layers, namely: lean clay crust, soft lean clay, and soft fat clay, were determined from the results of several triaxial tests (CU) and vane shear test (Han and Ye, 2006).

The elastic perfectly plastic stress-strain relationship incorporated with Mohr-Coulomb failure criterion is utilized to simulate the stress-strain behaviour of the soil. This material model is considered a reasonable approximation of the real non-linear stress-strain behaviour of soil. It requires five input parameters, namely: modulus of elasticity E, Poisson's ratio ν, and strength parameters c and ϕ, and dilatancy angle ψ. The micropile is modelled as a linear elastic material.

The soil is expected to display undrained behaviour because of the rapid rate of loading for the quick maintained load test. However, care must be taken into consideration when assigning the shear strength parameters of soft clays. As recommended by Brinkgreve (2001), the undrained shear strength parameters are used to reach a realistic stress path followed by the Mohr-Coulomb model for such type of soil. Consequently, the friction angle ϕ is set to 0 and the cohesion c is set to the undrained value C_u. Therefore, the results of the vane shear test are used to characterize the soil strength employing the idealized distribution with depth as shown in **Fig. 3**. For the available plasticity range, the correction factor for the vane test results is approximately 1.0 (Bjerrum's, 1972). The undrained shear strength, C_u, varies between 41.3 and 29 kPa for the lean clay crust, 29 kPa in the soft lean clay (1), and 35 kPa for the soft lean clay (2). The C_u of the soft fat clay (23.5 kPa) was estimated from the empirical correlation proposed by Gao (1994) for Shanghai clay based on its natural moisture content (50.8%), as follows:

$$C_u = 11 w_c^{-1.13} \qquad (2)$$

The modulus of elasticity of the soils was back-calculated from the results of plate load testing conducted on the surface of the clay crust and from the micropile loading test. The slow maintained plate load test yielded a value of 13.3 MPa for the drained modulus of elasticity E`, which is utilized to represent the stiffness of the lean clay crust and soft lean clay (1). On the other hand, a value

of 30 MPa was back-calculated for the undrained modulus of elasticity E_u for the soft lean clay layer. These values account for the effect of stress level, which in turn could approximately incorporate the influence of soil non-linearity. For high plastic clays, E_u is assumed to vary between 400 – 500 times C_u (Holtz and Kovacs, 1981). Consequently, a value of 10400 kPa was assigned to the soft fat clay. It is worth noting that in order to reach a reasonable assessment of the soil behaviour using Mohr-Coulomb model, the drained modulus of elasticity should be assigned. Therefore, the measured E_u is converted into the drained modulus E` through the theory of elasticity using drained Poisson's ratio $\nu`$ of 0.35, i.e.

$$E` = \frac{2}{3}(1+\nu`)E_u \qquad (3)$$

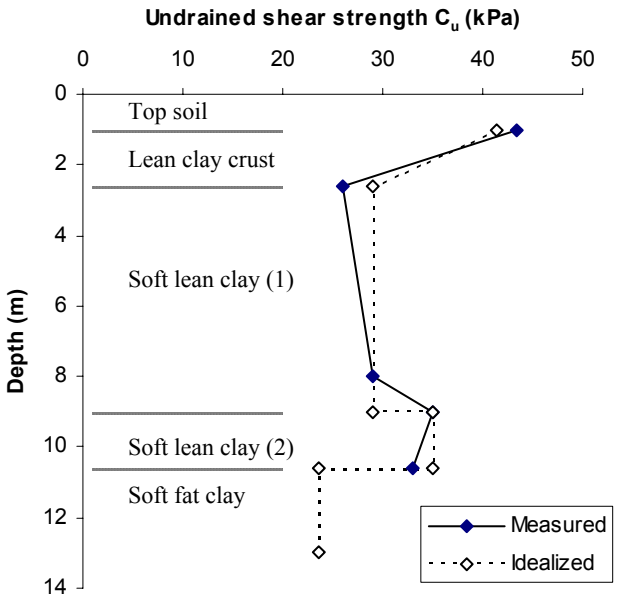

Figure 3. Measured and idealized distribution of the undrained shear strength.

The state of stress in soil after micropile installation is presumed to satisfy the at-rest condition. During the construction of the micropile, the stability of the drilled hole was maintained by providing jets of water to generate slurry from the soil. Such action has an adverse effect on the lateral stresses in soil at the interface with the micropile. Fortunately, it can be recovered by applying the grouting pressure (0.2 – 0.5 MPa), which in turn increases the coefficient of lateral earth-pressure K to a value slightly over the initial at-rest K_o. Contrariwise, the relaxation in stresses in the soft soils leads to the decline in K to reach the initial K_o. Mayne and Kulhawy (1982) proposed a correlation for calculating K_o based on the Jaky's simplified formula to account for the effect of the unloading portion of the stress path, as follows:

$$K_o = (1 - \sin\phi`)OCR^{\sin\phi`} \quad (4)$$

where, $\phi`$= the effective friction angle and OCR = the over-consolidation ratio. There was no available data in the reference study (Han and Ye, 2006) on the effective angle of friction of the site soils. Thus, the values of $\phi`$ were extracted from another study on the Shanghai soft clay by Schoeder et al. (1992). The values of $\phi`$ were 22, 17, and15 for the lean clay crust, soft lean clay, and soft fat clay, respectively. Schoerder et al. (1992) reported that these soils were normally consolidated except the upper crust had OCR = 5, which is considered moderately over-consolidated (O'Neil and Reese, 1999).

In order to model the excess pore water pressure dissipation during the consolidation stages, reasonable values for the coefficients of permeability for the soils need to be estimated. The vertical and horizontal coefficients of permeability, K_v and K_h, for the soft Shanghai clay were obtained from Shen et al. (2005). The field hydraulic conductivity has been estimated from laboratory results using the correlation developed by Tavenas et al. (1986):

$$\left(\frac{K_h}{K_v}\right)_{field} = C_f\left(\frac{K_h}{K_v}\right)_{laboratory} \quad (5)$$

where, C_f is proportionality factor = 6.0. The conductivity coefficients thus evaluated were $K_v = 2.55\text{x}10^{-9}$ m/sec and $K_h = 6.48\text{x}10^{-9}$ m/sec for the lean crust and $K_v = 1.85\text{x}10^{-9}$ m/sec and $K_h = 2.93\text{x}10^{-9}$ m/sec for the soft lean and fat clays. This leads to a horizontal to vertical coefficients ratio between 1.6 and 2.5, which is consistent with the ratios available in Lambe and Whitman (1979) for normally consolidated and slightly over-consolidated clays. Moreover, the permeability coefficients for the soft lean and fat clays are in good agreement with the range provided by Lambe and Whitman (1979) and Francis (1985) for vertical permeability (10^{-9} to 10^{-11} m/sec) in case of high liquid limit clays. It is noted that the adopted values in the current study are close to the higher limit (10^{-9} m/sec) since the soils contained an appreciable fraction of silt. **Table 1** provides the soil and micropile material properties adopted in the numerical model.

The interface element used can bridge two different element types and transfers only shear stress by friction. It is, therefore, assigned to simulate the intensely sheared zone between the pile and the surrounding soil. The elastic-perfectly plastic model is utilized to describe the behaviour of the interface. The strength properties of the interface are linked to the strength properties of the corresponding soil layer by introducing a strength reduction factor R_{int}. Consequently, the interface properties are calculated as follows:

$$C_i = R_{int}C_u \quad (5)$$

where, C_i = interface cohesion. The value of R_{int} is varied in the analysis to reach favourable match between the simulated and measured load-displacement curves.

Table 1. Adopted soil properties for modelling.

Note: γ_d =unit weight above water level.

	Lean clay crust	Soft lean clay (1)	Soft lean clay (2)	Soft fat clay	Micropile
Model	Mohr-Coulomb	Mohr-Coulomb	Mohr-Coulomb	Mohr-Coulomb	Linear-Elastic
Behaviour	Undrained	Undrained	Undrained	Undrained	Non-porous
γ_d (kN/m^3)	19.1	17.6	17.6	17.1	23.6
γ_{sat} (kN/m^3)	19.1	17.6	17.6	17.1	-
C (kPa)	41.3-29	29	35	23.5	-
ϕ^o	0	0	0	0	-
E` (MPa)	13.30	13.30	27	9.40	31400
ψ^o	0	0	0	0	-
ν`	0.35	0.35	0.35	0.35	0.15
K_v (m/sec)	2.55×10^{-9}	1.85×10^{-9}	1.85×10^{-9}	1.85×10^{-9}	-
K_h (m/sec)	6.48×10^{-9}	2.93×10^{-9}	2.93×10^{-9}	2.93×10^{-9}	-
R_{int}	Variable	Variable	variable	variable	-

EVALUATION OF INTERFACE CHARACTERISTICS BY BACK-ANALYSIS

The current practice adopts the total stress analysis for computing the shaft capacity of piles, using data mostly related to large diameter drilled and driven piles. In such type of analysis, the shaft resistance F_s is related to the undrained soil strength C_u through the adhesion factor α, i.e.

$$F_s = \alpha . C_u \qquad (6)$$

However, due to the micropile small diameter and construction techniques, the empirically obtained α values for large diameter piles may not be valid for micropiles. Thus, two methodologies have been adopted to arrive at a reliable quantification of α value and minimize the discrepancy for micropiles applications in soft clays (see **Fig. 4**). Numerically, the interface strength reduction factor R_{int} is considered a representation of the adhesion factor α as it reflects the load transfer mechanism along the micropile shaft.

In the first methodology, the soil parameters determined in the reference study are maintained, and the R_{int} value is altered to reach the best agreement between the simulated and field measured response curves. In the second methodology, a reasonable level of uncertainty is imposed on the measured soil

parameters, to back-calculate lower and upper bounds for the R_{int} value. For consistency with conventional terminology for describing shaft resistance, the term α will be used to stand for R_{int} in the rest of the paper.

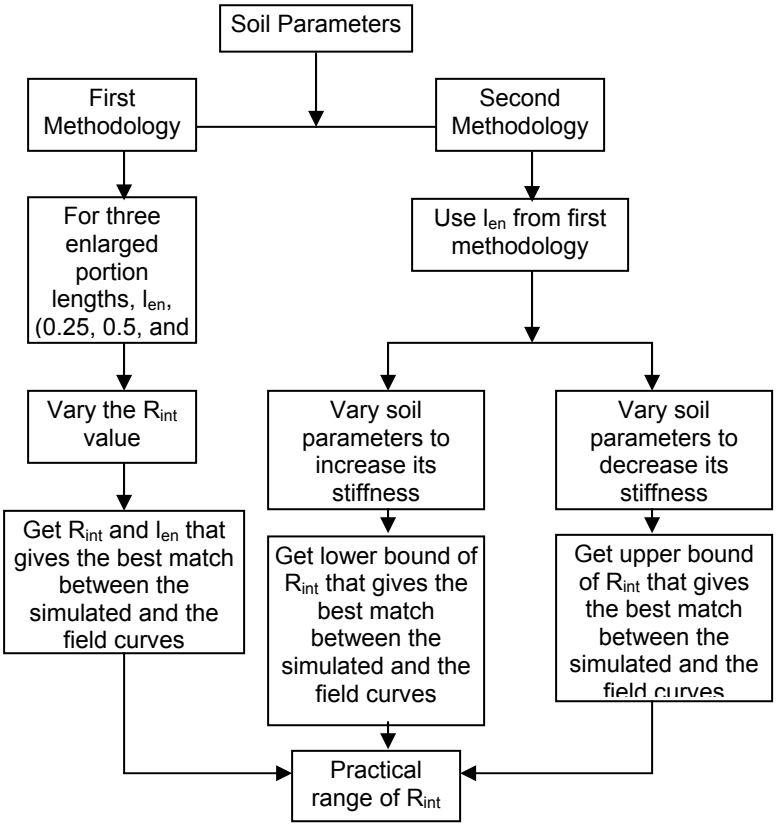

Fig. 4. Flow chart for R_{int} evaluation.

First Methodology

It is believed that the conducted laboratory and field tests were well-controlled. Thus, the adopted soil parameters in **Table 1** are presumed to be reasonably reliable for estimating α value for the analyzed micropile. Three rounds of analysis have been implemented to investigate the effect of the enlarged base of the micropile considering the previously specified enlarged lengths (l_{en} = 0.25, 0.5, and 1.0m). For each round, a value of α is obtained. Based on the monitored behaviour, a single case from the aforementioned three rounds would be selected to be representative of the actual geometry of the micropile. Consequently, its relevant α value is deemed to be the best estimate.

The load-displacement curves for the tested micropile are reported in **Fig. 5**. The value of α has been varied between 0.8 and 1.0 to match the field curve. The examination of the figure reveals that the best estimate of α is 0.9 and the length of the enlarged portion of the micropile had a minor influence on the

calculated curves. This value is higher than the upper bound of the α range (0.6 – 0.8) recommended by Bruce (1994). It is also seen that the ultimate load has been attained in both the simulated and measured curves defined by the plunging failure occurred at a load of 135 kN.

The load sharing mechanism between the shaft and toe resistances is provided in **Fig. 6** and **Table 2**. It can be concluded that the estimated load sharing mechanism is in favourable agreement with the measured values, especially cases 2 and 3. In **Fig. 6**, the axial load distribution in micropile is plotted at 50, 75, and 100% of the ultimate load. Again, the agreement is quite satisfactorily between the estimated and measured curves with some discrepancy near the end of the micropile at the ultimate load. It should be noted that the experimental curves do not reflect the exact distribution because of the limited number of strain gauges attached to the reinforcing cage. The results of the numerical analysis showed a slight increase in the axial load near the end. This can be attributed to considering the enlarged portion, resulting in a different load sharing mechanism at the end of the micropile. Thus, the enlarged grouted part mobilized negative skin friction, a phenomenon that has been observed by Russo (2004). The recorded abrupt increase in axial load decreased with depth until it reached the micropile toe. Examining the calculated response of the micropiles for cases 1, 2, and 3, it can be concluded that the geometrical configurations of case 3 is closest to field conditions.

The toe resistance evaluated from both field measurements and numerical analysis of case 3 is about 8-9% of the micropile capacity, confirming that small toe resistance may be mobilised by micropiles, as observed by many researchers (Koreck, 1978; Bruce, 1994; Bruce and Juran, 1997). This is demonstrated by the abrupt failure when the maximum resistance was reached after small displacements (usually 20 to 40 times less than those needed to mobilise end bearing). In addition, the mobilised portion of the toe resistance was found to be 9% of the shaft resistance, which is compatible with the upper bound (15 – 20%) provided by Bustamanti and Diox (1985). In order to identify the failure pattern on the numerical model, the development of the Mohr-Coulomb failure points is monitored during the successive load increments. It was observed that the failure initiated at the toe of the micropile and expanded upward and laterally along the shaft with the increase of the applied load.

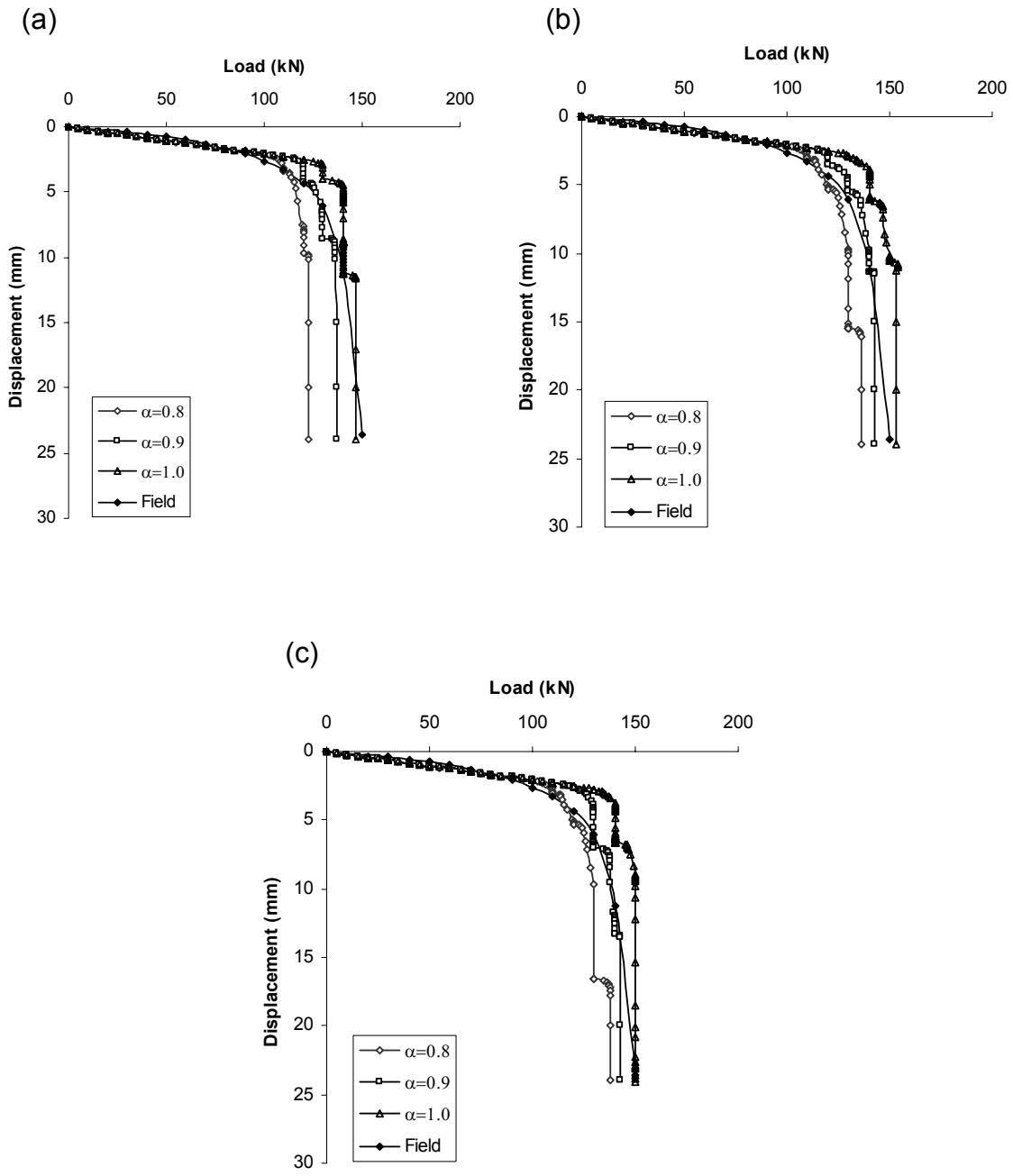

Fig. 5. Field and simulated load-displacement curves for enlarged portion length of: (a) 0.25m; (b) 0.5m; (c) 1.0m.

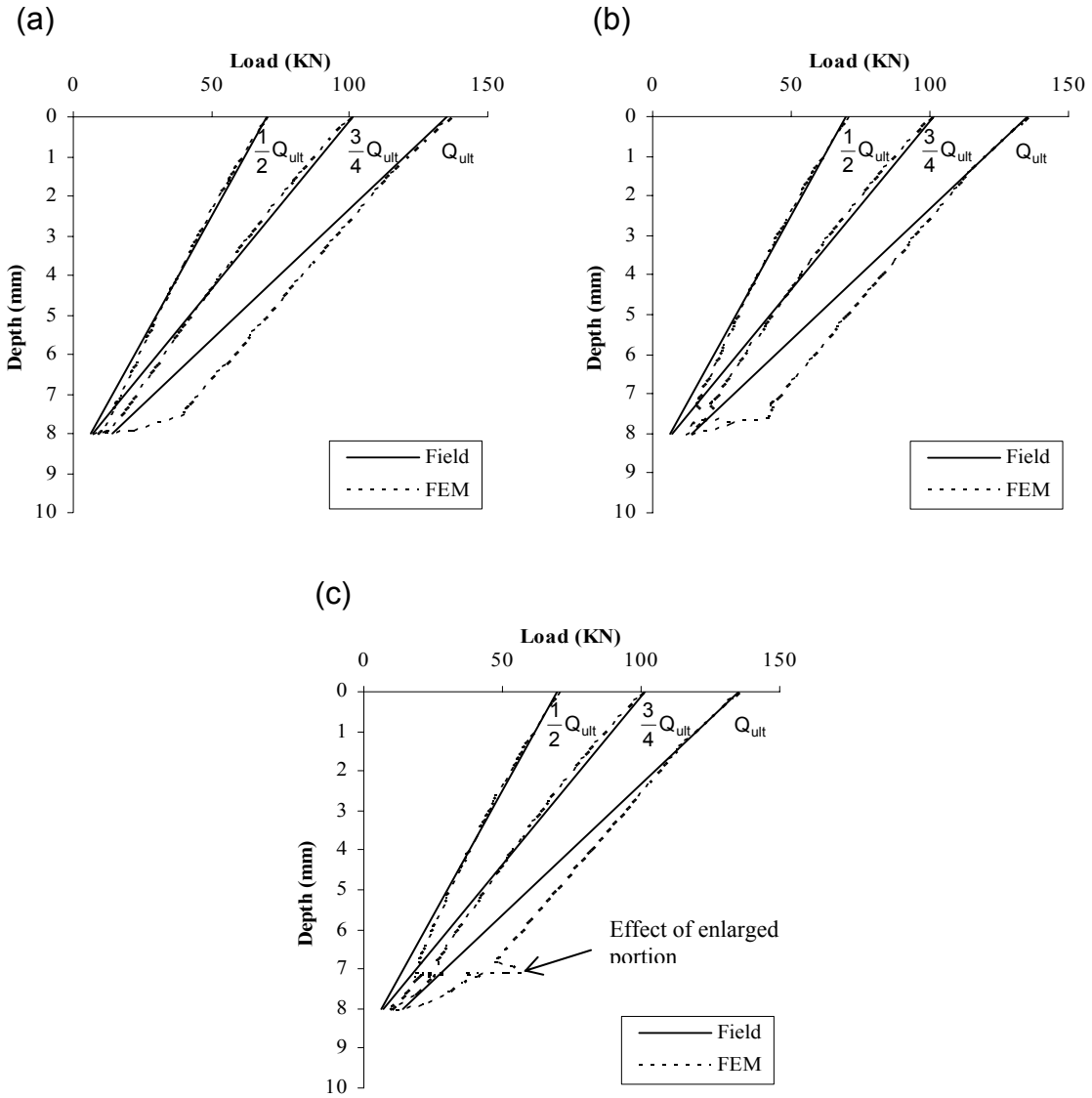

Fig. 6. Field and simulated axial load in micropile for enlarged portion length of: (a) 0.25m; (b) 0.5m; (c) 1.0m.

Table 2. Load sharing values.

Case	Enlarged portion length l_{en} (m)	Ultimate load (kN)	Toe resistance (kN)	Shaft resistance (kN)	% Toe resistance	% Shaft resistance
1	0.25	135	6.0	129	4.5	95.5
2	0.5		13.8	121.2	10.2	89.8
3	1.0		11.0	124	8.0	92.0
field	-		11.7	123.2	8.7	91.3

Second Methodology

In order to establish lower and upper bounds of α accounting for the uncertainty of the soil parameters, additional analysis are performed considering the nominal soil parameters ± 10%. The lower bound is obtained by increasing the soil undrained shear strength and elastic modulus. The results of the analysis are illustrated in **Fig. 7a**, showing a lower bound of α = 0.8. The upper bound of α is estimated by decreasing the soil E` and C_u values by 10%. This analysis resulted in upper bound of α = 1.0 (see **Fig. 7b**). These results show that α can be higher than the values recommended by Bruce (1994).

EFFECT OF SHAFT DIAMETER

To investigate the effect of the shaft diameter on the estimated ultimate load and load sharing mechanism, three sets of analysis are performed. The diameter of the micropile shaft, above the enlarged base, is increased from 0.15 m to 0.17, 0.19, and 0.228 m. Whereas, the last adopted diameter displays the case of micropile of uniform cross section without enlarged base. These analysis are performed by incorporating the previously obtained best estimate of α = 0.9.

Figures 8 and 9 and Table 3 show the results of these analyses. It is observed that all cases experienced plunging failure with the ultimate loads exceeding the reference value by 11, 21, and 34% for diameters 0.17, 0.19, and 0.228 m, respectively. These results demonstrate a linear relationship between the pile diameter and its capacity. The unit shaft resistance was almost constant, which agrees satisfactorily with the parametric study done by Frassetto (2004). It is worth noting that the calculated unit shaft resistances represent the ultimate values as a consequence of shear failure along the micropile-soil interface. This means that no progressive failure mechanism has occurred along the interface. The axial load in the micropile displayed the same distribution for all studied cases. The effect of negative skin friction due to the enlarged base diminished after increasing the diameter to 0.19 m, as the difference in diameter between the micropile shaft and the enlarged base decreased.

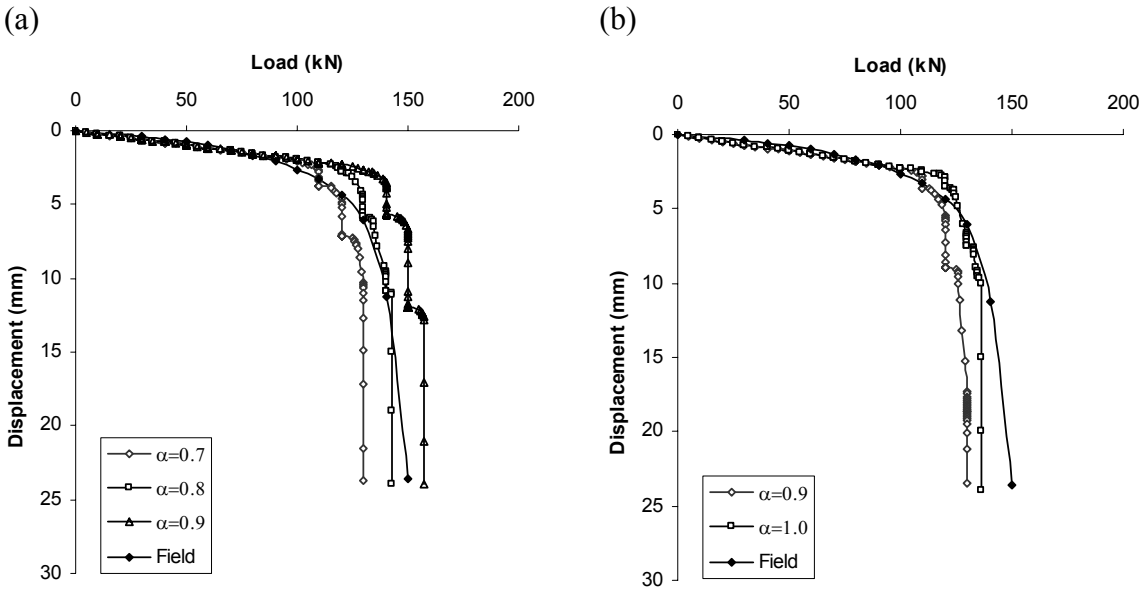

Fig. 7. Field and simulated load-displacement curves for: (a) lower bound of α; (b) upper boud of α.

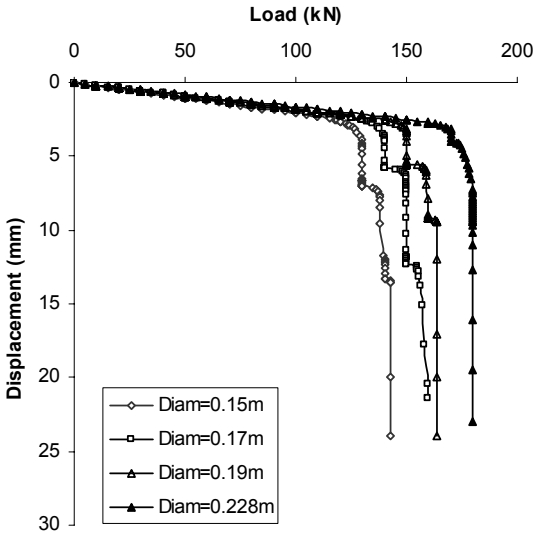

Fig. 8. Load-displacement curves for different micropile shaft diameters.

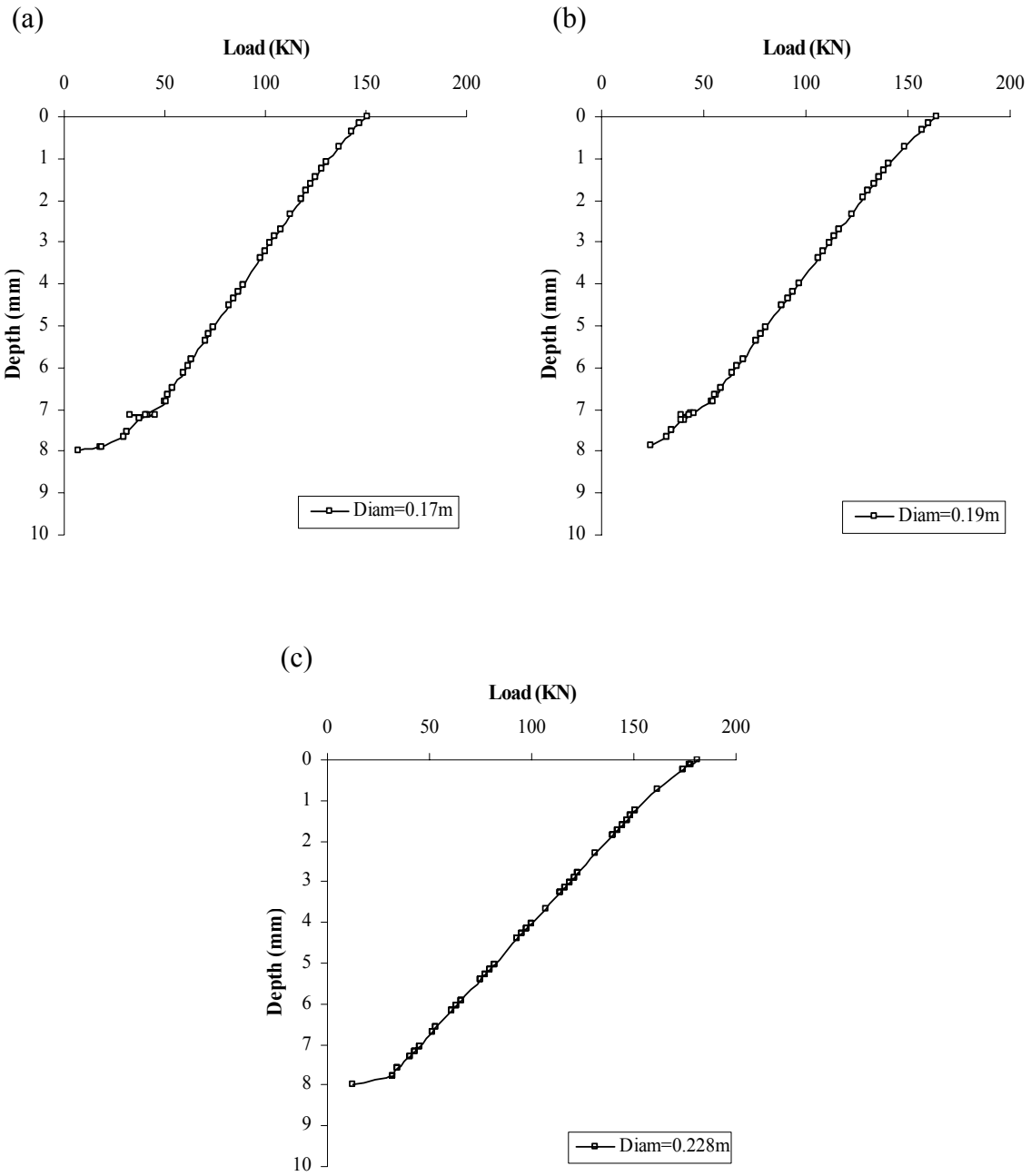

Fig. 9. Axial load in micropile: (a) diameter=0.17 m; (b) diameter=0.19 m; (c) diameter=0.228 m.

Table 3. Effect of micropile diameter on load sharing mechanism.

Case	Diameter (m)	Ultimate load (kN)	Toe resistance (kN)	Shaft resistance (kN)	% increase in ultimate load	Unit shaft resistance (kPa)
1	0.15	135	11	124	-	30.8
2	0.17	150	7.3	142.7	11	32
3	0.19	163	8.8	154.5	21	31.5
4	0.228	181	12.6	168.4	34	29.5

CONCLUSIONS

The behaviour of a single isolated micropile in soft clayey soils was investigated. Inverse analysis was performed to investigate the adhesion characteristics of the micropile-soil using a coupled two-dimensional finite element analysis. Two methodologies were considered to establish an adequate quantification of the adhesion factor α. Moreover, the effects of the micropile diameter on the mobilized ultimate resistance and load sharing mechanism were investigated. The following conclusions can be drawn:

1. The estimated range of the adhesion factor α was between 0.8 and 1.0, with the best estimate of 0.9. This is higher than the range 0.6-0.8 proposed by Bruce (1994).
2. The values of α are site specific and highly dependent on the construction technique, type of micropile, and many other factors. Thus, this study aims at giving indicative values of α for more optimized designs.
3. The use of large grouted volume in the lower part of the micropile can mobilize some negative skin friction.
4. The failure of soft clay soils surrounding the micropile was initiated at the toe and expanded upward and laterally along the shaft.
5. The increase in shaft diameter relative to the diameter of the enlarged base eliminated the negative skin friction.
6. The ultimate capacity of the micropile increased approximately linearly with the increase in the shaft diameter. The load sharing mechanism, however, remained the same.

NOTATIONS

c	Total cohesion;
C_f	Proportionality factor (C_f =6.0);
C_i	Interface cohesion;
C_u	Undrained cohesion;
E`	Drained modulus of elasticity;
E_u	Undrained modulus of elasticity;
K	Coefficient of lateral earth-pressure;

K_h	Horizontal coefficient of permeability;
K_o	Coefficient of lateral earth-pressure at-rest;
K_v	vertical coefficient of permeability;
L	Micropile length;
l_{en}	Enlarged portion length;
I_l	Liquidity index;
OCR	Over-consolidation ratio;
PL	Plastic limit;
R	Radius at which the shear stress becomes negligible;
R_{in}	Interface strength reduction factor;
r_m	Micropile mean radius;
w_c	Moisture content;
α	Adhesion factor;
ϕ	Total friction angle;
$\phi`$	Effective friction angle;
γ_d	unit weight above water level;
γ_{sat}	Saturated unit weight;
ν	Undrained Poisson's ratio; and
$\nu`$	Drained Poisson's ratio;

REFERENCES

ASTM (1987). Standard test method for piles under static axial compressive load. ASTM D1143-81. In Annual Book of ASTM Standards, 04.08. American Society of Testing and Materials: 194-204.

Bjerrum, L., (1972). Embankments on soft ground, Proceedings of the ASCE Speciality Conference on Performance of Earth and Earth-Supported Structures, Purdue University, Vol. 2: 1-54.

Brinkgreve, R. B. J., (2001). 2D-Plaxis version 8 manual, Delft University Technology and Plaxis b.v., The Netherlands.

Bruce, D.A., and Yeung, C.K., (1983). A review of minipiling, with particular regard to Hong Kong applications, Hong Kong Engineering, 12(6): 31-54.

Bruce, D.A., (1988). Aspects of minipiling practice in the United States, Ground Engineering, 21(8): 20-33.

Bruce, D.A., (1989). Aspects of minipiling practice in the United States, Ground Engineering, 22(1): 35-39.

Bruce, D.A., (1994). Small-diameter cast-in-place elements for load bearing and in situ earth reinforcement, Chapter 6 in Ground Control and Improvement by P.P. Xanthakos, L.W. Abramson, and D.A. Bruce, John Wiley and Sons.

Bruce, D.A., and Juran, I., (1997). Drilled and grouted micropiles: state-of-practice review, Federal Highway Administration, Washington, D.C. FHWA-RD-96-017.

Bustamante, M., and Diox, B., (1985). Une Méthode pour le calcul des micropieux injectes, Bulletin de Liaison des Laboratoires des Ponts et Chaussées, LCPC, Paris: 75-92.

Frassetto, J.C., (2004). Performance of micropiles, M.Sc. Thesis, Concordia University, Canada.

Gao, D.Z., (1994). Ultimate bearing capacity of soft soil, Proceedings of the 7th Chinese Soil Mechanics and Foundation Engineering Conference: 300-304 (in Chinese).

Han, J., and Ye, S., (2006). A field study on the behavior of micropiles in clay under compression or tension, Canadian Geotechnical Journal, 43(1): 19-29.

Holtz, R.D., and Kovacs, W.D., (1981). An introduction to geotechnical engineering, Prentice-Hall, Inc, USA.

Jeon, S., (2004). Interpretation of load tests on micropiles, Geotechnical Engineering, ICE, 157(GE2): 85-90.

Juran, I., Bruce, D.A., DiMillio, A.F., and Benslimane, A., (1999). Micropiles: the state of practice. Part II: design of single micropiles and groups and networks of micropiles, Ground Improvement, 3: 89-110.

Koreck, H.W., (1978). Small diameter bored injection piles, Ground Engineering, 11(4): 14-20.

Lambe, T.W., and Whitman, R.V., (1979). Soil mechanics, John Wiley & Sons, Inc, Toronto.

Littlejohn, G.S., (1980). Design estimation of the ultimate load-holding capacity of ground anchors, Ground Engineering, 13(8): 25-39.

Lizzi, F., (1985). The pali radice (root piles) and reticulated pali radic, Underpinning, Surrey University Press: 84-151.

Mason, J.A, and Bruce, D.A., (2001). Lizzi's structural system retrofit with reticulated internal reinforcement method, Traansportation Research Record, No. 1772: 107-114.

Mayne, P.W., and Kulhawy, F.H., (1982). K_o – OCR relationships in soil, Journal of Geotechnical Engineering Division, ASCE, 108(GT6): 851-872.

O'Neill, M.W., and Reese, L.C., (1999). Drilled shafts: construction procedures and design methods, Federal Highway Administration, Washington, D.C., FHWA-IF-99-025.

Randolph, M.F., and Wroth, C.P., (1978). Analysis of deformation of vertically loaded piles, Journal of Geotechnical Engineering, ASCE, **114**(12): 1465-1488.

Randolph, M.F., (1994). Design methods for pile groups and piled rafts, Proceedings of the 13th International Conference on Soil Mechanics and Foundation Engineering, New Delhi, India, Vol. 5: 61-82.

Russo, G., (2004). Full-scale tests on instrumented micropiles, Geotechnical Engineering, ICE, 157(GE3): 127-135.

Schroeder, C.H., Dassargues, A., and Li, X.L., (1992). Engineering geological condition in the central area of Shanghai, Bulletin of the international Association of Engineering Geology, No. 46, Paris: 35-41.

Shen, S.L., Chai, J.C., Homg, Z.S., and Cai, F.X., (2005). Analysis of field performance of embankments on soft clay deposit with and without PVD-improvement, Journal of Geotextiles and Geomembranes, 23(6): 463-485.

Tavenas, F., Tremblay, M., Larouche, G., and Leroieil, S., (1986). In-situ measurement of permeability in soft clays, ASCE Special Conference on Use of In-situ Tests in Geotechnical Engineering. ASCE, New York: 1034–1048.